Available online at www.sciencedirect.com
ScienceDirect
Ceramics International 33 (2007) 1223–1229
CERAMICS INTERNATIONAL
www.elsevier.com/locate/ceramint

Microstructure and electrical properties of Si_3N_4–TiN composites sintered by hot pressing and spark plasma sintering

Zhiquan Guo [a], Gurdial Blugan [a], René Kirchner [c], Mike Reece [b], Thomas Graule [a], Jakob Kuebler [a,*]

[a] *Empa, Material Science & Technology, Laboratory for High Performance Ceramics, Ueberlandstrasse 129, Duebendorf, CH-8600, Switzerland*
[b] *Queen Mary, University of London, Mile End Road, London E2 4NS, UK*
[c] *FCT Systeme GmbH, Gewerbepark 11, 96528 Rauenstein, Germany*

Received 29 December 2005; received in revised form 10 March 2006; accepted 30 March 2006
Available online 1 September 2006

Abstract

Electroconductive Si_3N_4–TiN composites were fabricated from micron-sized Si_3N_4 and nano-sized TiN powders by powder processing routes. The specimens were consolidated by hot pressing (HP) and spark plasma sintering (SPS). High densities (>98%) were obtained by sintering at temperatures ≥1500 °C using both sintering methods. The TiN phase grows rapidly during the liquid phase sintering, and its grain size increases with sintering temperature, leading to the increase in electrical resistivity. Dense materials produced by SPS possess significantly higher resistivity than the hot-pressed materials due to the larger TiN grain size and the presence of crystallized grain boundary phase.

Keywords: D. Si_3N_4; A. Hot pressing; B. Composites; C. Electrical properties

1. Introduction

Silicon nitride (Si_3N_4) is an important high temperature structural ceramic due to its excellent combination of mechanical properties and thermal stability. However, like most ceramics, its brittle nature has limited its application. Addition of electroconductive particles, such as TiN [1], TiB_2 [2], $MoSi_2$ [3,4], etc., to the insulating Si_3N_4 matrix can toughen the materials by mechanisms, including residual stresses and crack deflection [1,5]. Moreover, inclusion of these above mentioned interconnected conductive particles in the composites provides high electron conductivity, which allows Si_3N_4 based materials to be manufactured into complex shapes by electrical discharge machining (EDM) at relatively low cost. A commercial Si_3N_4–TiN composite, under the name of Syalon 501, was developed for this purpose [6]. In addition, conductive TiN–sialon composites were also synthesized by in situ reaction [7] or phase mixing [8]. The reduction of the conductive particle size can lead to an improvement in corrosion resistance [9] and lower the percolation concentration [1]. The trend should continue if the conductive particles are reduced to the nano scale.

Nano-sized TiN particle containing Si_3N_4 composites can be synthesized by mechano-chemical grinding (MCG) of Si_3N_4 and Ti metal in N_2 atmosphere [10] or by coating nano-sized TiN particles on Si_3N_4 powders, which are prepared through a chemical route [11]. However, due to the complexity of these processing techniques, they are not suitable for large-scale production. Limited effort [12] has been made to fabricate electroconductive Si_3N_4–TiN composites from nano powders via conventional powder processing route.

Generally, Si_3N_4–TiN materials can be consolidated by hot pressing (HP) [1,13,14]. However, significant grain growth of TiN phase was observed in HPed Si_3N_4–TiN nanocomposites [12]. This is probably because of the low heating rates used and long sintering times required to obtain full density. An alternative sintering technique, namely spark plasma sintering (SPS), has attracted considerable attention. It is closely related to conventional hot pressing; the fundamental difference is that heat is generated internally by a pulsed current passing through

* Corresponding author. Tel.: +41 44 8234223; fax: +41 44 8234150.
E-mail address: jakob.kuebler@empa.ch (J. Kuebler).

0272-8842/$32.00
doi:10.1016/j.ceramint.2006.03.029

a graphite die and also through the powder compacts in the case of conductive specimens. This technique offers a unique combination of rapid heating/cooling and shorter processing times, which makes it an interesting tool to consolidate nanopowders and retain nanostructures [15]. SPS has been utilized to densify the Si_3N_4–TiN nanocomposites and highly conductive composites ($\sim 10^{-3}\ \Omega$ cm) with submicron-sized TiN grain were obtained [11,16]. However, to our knowledge, there has been no study on the difference in the sintering behaviours of Si_3N_4–TiN produced by HP and SPS.

In this paper, we report the preparation of electroconductive Si_3N_4–TiN composites from Si_3N_4 and nano-TiN powders using conventional powder processing. Materials were consolidated by HP and SPS. The influences of sintering techniques and temperature on microstructure and electrical resistivity of the composites were studied.

2. Experimental procedure

The starting powders were characterised in terms of specific surface area (SSA) using a surface area analyzer (SA 3100, Coulter) and absolute density by a He-Pycnometer (AccPyc 1330, Micromeritics).

Commercial Si_3N_4 powder (grade M11, H.C. Starck, Germany) with 2.5 wt.% Al_2O_3 (CT3000 SG, Bassermann Minerals, Germany) and 4.5 wt.% Y_2O_3 (grade C, H.C. Starck, Germany) were used to prepare the precursor powder. In addition, 41.4 wt.% (= 30 vol.%) of nano-sized TiN powder (Plasma & Ceramic Technologies, Latvia) was added as the conductive phase. 3.7 wt.% dispersant–SOLSPERSE 20000 (Noveon, England) was added to the powder mixture dispersed in isopropanol. The starting powders were mixed by a planetary mill (PM400, Retsch) at a rotation speed of 300 rpm for 16 h using a 500 ml Al_2O_3 jar with 2.5 mm Al_2O_3 balls. The particle size distribution in the suspension was measured by a laser diffraction particle size analyzer (LS230, Beckman Coulter) after every 4 h of milling. The powder mixture was dried in a rotary evaporator and passed through a 200 μm sieve. The dried powder was heated at 400 °C for 1 h in a N_2 atmosphere to remove the residual organics after granulation. Disc-shaped green bodies with a diameter of 15 mm, prepared by uniaxial pressing, were used for hot pressing (Model 383-40, Thermal Technology Inc.) in the temperature range of 1400–1700 °C with 10 min dwell time and under a pressure of 30 MPa in 1 atm N_2 atmosphere. Loose powder was used for SPS (HPD-25, FCT Systeme GmbH, Germany). The SPS experiments were carried out in the temperature range of 1400–1600 °C with a 10-min dwell time and under 100 MPa uniaxial pressure. The heating rates were 80 and 200 °C/min for HP and SPS, respectively. In both cases, the temperature was monitored by an optical pyrometer.

The measured densities of the starting powders were used to calculate the theoretical density of the composites by rule of mixture, assuming no reaction had taken place between the components. The effective densities of the sintered composites were measured by Archimedes principle. The cross-sections of the sintered samples were polished and plasma etched for microstructural characterisation by scanning electron microscope (SEM) (JEOL JSM-6300F). Transmission electron microscope (TEM) (JEOL JEM-2010) was used to characterise the morphology of the nano TiN powder and the microstructures of the sintered samples. Phase identification was performed by an X-ray diffractometer (XRD) (PANalytical PW 3040/60 X'Pert PRO) with Ni-filtered Cu Kα radiation of wavelength 1.5418 Å ($5^\circ \leq 2\theta \leq 80^\circ$). The electrical resistivity of the composites was measured at room temperature by the four-probe van der Pauw method [17].

3. Results and discussion

3.1. Powder characterisation

The characteristics of the starting powders are summarized in Table 1. The measured densities of Si_3N_4, Y_2O_3 and Al_2O_3 are comparable with their theoretical densities [18]. However, the density of TiN nanopowder is about 8% smaller than the theoretical one (5.29 g/cm^3) [18]. It is believed that the low density of TiN powder is due to the absorption of oxygen (1.8%) and subsequent formation of TiO_2 on the surface. This was confirmed by XRD, which reveals that the TiN nanopowder mainly contains osbornite (TiN) phase with traces of rutile (TiO_2) phase. On the other hand, the Si_3N_4 powder mainly consists of α-Si_3N_4 (>90%) with a small amount of β-Si_3N_4. Fig. 1 shows the morphology of the as-received TiN nanopowder. The TiN nanoparticles appear as cubic and triangular shapes, which have the same electron diffraction patterns and thus the same crystal lattice structure. According to TEM image, the primary particle size of TiN nanopowder is approximate 45 nm, which is in good agreement with the value calculated from SSA (~48 nm). Due to the large surface area, as-received TiN nanoparticles were agglomerated into particle clusters with a diameter up to several microns.

3.2. Processing, densification and phase composition

Homogenisation is a critical step in powder processing. Inadequate homogenisation can lead to agglomeration of added second-phase particles in composite materials, which might result in e.g. degradation in electrical conductivity [19] and mechanical properties [1]. This problem becomes even more

Table 1
Characteristics of starting powders

	SSA (m^2/g)[a]	Density (g/cm^3)[b]	Phase composition[c]	Oxygen content (%)[d]
Si_3N_4	14.0	3.22	>90% α-Si_3N_4, β-Si_3N_4	1.4
TiN	25.6	4.87	Osbornite, rutile	1.8
Y_2O_3	8.0	4.66	Crystalline	–
Al_2O_3	12.4	3.88	Corundum	–

[a] Measured by BET.
[b] Measured by He-Pycnometer.
[c] Measured by XRD.
[d] Supplier specification.

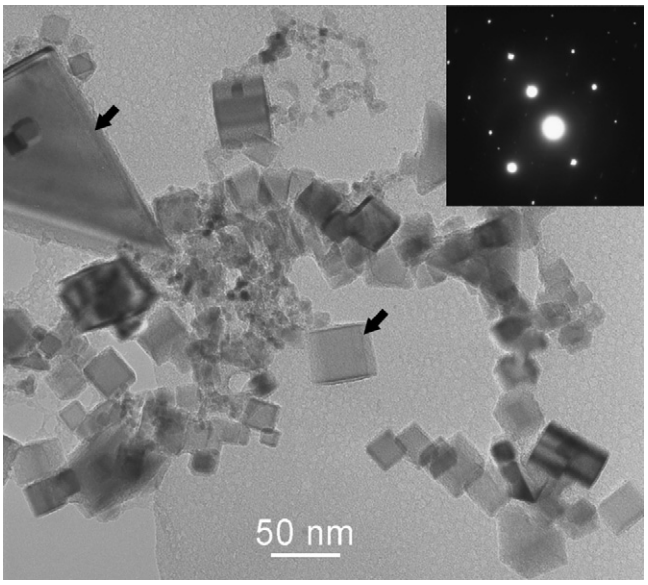

Fig. 1. TEM micrograph and diffraction pattern of the as-received TiN nanoparticles.

pronounced, if the second phase is in the nanometre scale. High-speed planetary ball milling was employed to provide sufficient energy for deagglomeration and homogenisation of the powder mixture. Fig. 2 shows the particle size distribution of the suspension of the powder mixture as a function of milling time. The particle size distribution became narrower and the median particle size (d_{50}) decreased from 1.09 to 0.47 μm as a result of milling for 16 h; the large agglomerates (>1 μm) were totally removed. For comparison, a batch of TiN nanopowder was milled under the same condition and the particle size distribution is presented in Fig. 3. Similar to the powder mixture, the median particle size of TiN was reduced from 0.82 to 0.54 μm. It indicates that the planetary milling is effective to reduce the particle size for both micron-sized Si_3N_4 and nano-sized TiN powder.

The dried powders of 30 vol.% nano-TiN/Si_3N_4 were sintered with 10 min dwell time at different temperatures by

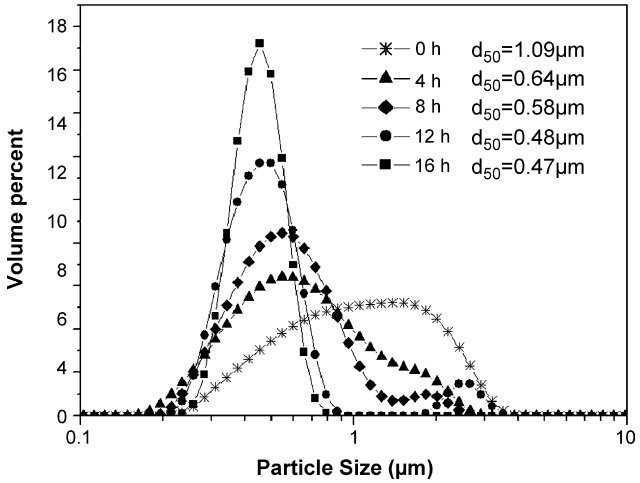

Fig. 2. Particle size distribution of suspension of Si_3N_4–TiN powder mixture as a function of milling time.

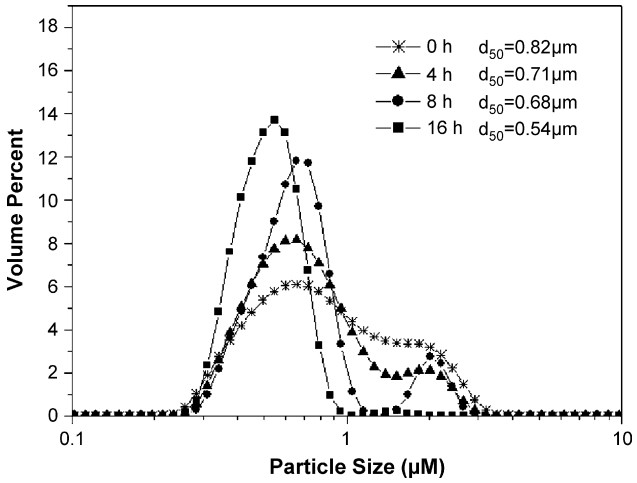

Fig. 3. Particle size distribution of suspension of TiN nano powder as a function of milling time.

HP and SPS. The relative densities of the sintered ceramics are shown in Fig. 4. It can be seen that the sintered densities of the specimens sintered between 1500 and 1700 °C by either methods are higher than 98%. These findings are in good agreement with the results in Gao's study [19], which were obtained by HP at temperatures above 1550 °C. Similar result was obtained in Si_3N_4–TiB_2 composites [15]. When sintering at 1400 °C, the relative densities are 78.0% and 86.6% for HP and SPS samples, respectively. The influence of the consolidation methods on the densification process cannot be directly clarified in the present study because different pressures were used in HP (30 MPa) and SPS (100 MPa).

The typical XRD patterns of sintered materials and as-received TiN nanopowder are shown in Fig. 5. In addition to the β-Si_3N_4 and TiN phases, α-Si_3N_4 phase was also identified in all sintered composites. As expected the β-Si_3N_4 content in the composites increased with the sintering temperature. However, complete α/β phase transformation of Si_3N_4 did not occur in either sintering method due to the short dwell time and the relatively low sintering temperatures used. Perera et al. reported that complete conversion to β phase only occurs at 1900 °C with a 5-min dwell time using SPS processing [20]. No diffraction peaks from other intermediate reaction compounds,

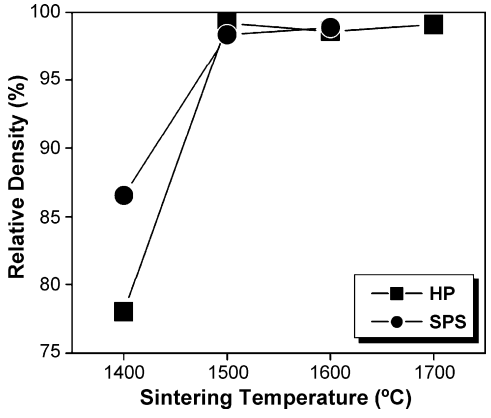

Fig. 4. Relative densities of samples sintered by HP and SPS.

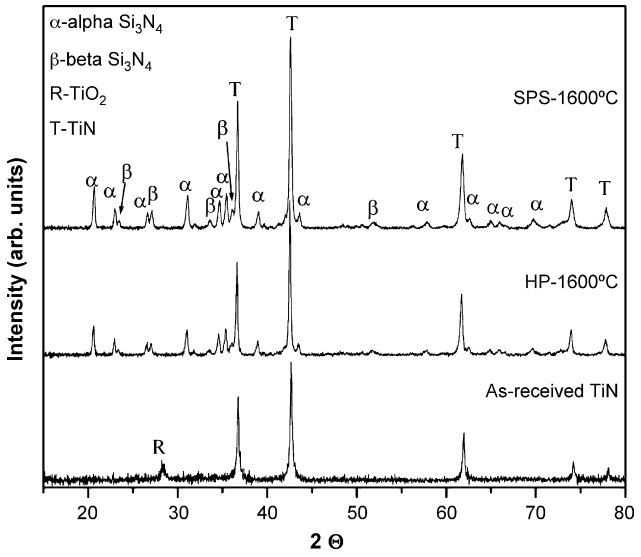

Fig. 5. XRD patterns of samples sintered at 1600 °C by HP and SPS, respectively, and for the as–received TiN nanopowder.

e.g. $TiSi_2$, were detected by XRD. This is consistent with the findings of Blugan et al. [5]. The phase composition, in terms of α- and β-Si_3N_4 and TiN contents, for both HP and SPS composites are similar. No influence of the sintering methods on the phase compositions was distinguishable by XRD.

3.3. Microstructure and electrical properties

Fig. 6 presents a comparison of microstructures of samples consolidated by HP and SPS at different sintering temperatures. The Si_3N_4 grains have an equiaxial shape and the grain size is in the range 0.1–1 μm, independent of sintering temperatures and processing methods. Typical elongated β-Si_3N_4 grains were not observed. According to the classical theory for the liquid phase sintering of Si_3N_4 proposed by Kingery [21], the coarsening of Si_3N_4 phase is the final stage of the liquid phase sintering and it normally takes place after the completion of the α/β phase transformation. However, for all sintered composites in present study, the α/β transformation was not completed even at highest sintering temperatures (1700 °C) used and therefore significant growth of β-Si_3N_4 grains was not possible. It has been reported that temperatures ≥1750 °C are required to produce elongated β-Si_3N_4 grains by SPS [20]. In addition, the dwell time of 10 min is too short to allow the β-Si_3N_4 grains to elongate significantly.

The TiN particles are distributed homogenously in the Si_3N_4 matrix. However, most of the TiN grains are in the submicron scale, which is much larger than the size of the starting nanopowder. Considering the high volume fraction (30 vol.%) of TiN nanoparticles in the composites and the powder packing, it is reasonable to expect that TiN nanoparticles located between large Si_3N_4 grains were stacked together and coarsened during sintering. Furthermore, the sintering temperatures show significant influence on the size of TiN grains. Fig. 7 shows the average TiN grain sizes as a function of sintering temperature, measured using the linear intercept method as described in standard EN 623-3 [22]. In the HP materials average TiN grain size increased from 0.27 to 0.74 μm (Fig. 6a–d) with increasing sintering temperature from 1400 to 1700 °C, which indicates that TiN nanoparticles coalesce and grow during liquid phase sintering. It has been reported that TiO_2 on the surface of the TiN nanoparticles can promote the formation of liquid phase at early sintering stage via the reaction (1) and TiN grains grow through solution and precipitation process [12,23].

$$3TiO_2 + Si_3N_4 \rightarrow 3SiO_2 + 3TiN + 0.5N_2 \quad (1)$$

It has been reported that a volume fraction of 30% of conductive TiN phase in the composites is above the percolation threshold [24] and the electrical conductivity of the composites is provided by the TiN network. This is supported by the current result. The correlation between electrical resistivity and sintering temperature is shown in Fig. 8. The change in electrical resistivity with sintering temperature is related to the evolution of the microstructure of the composites. For the dense HP samples, lowering the sintering temperature from 1700 to 1500 °C resulted in a decrease in resistivity from 0.18 to 0.004 Ω cm. According to the geometrical percolation model presented by Malliaris and Turner [25], the percolation threshold (V_c) of a composite is determined by the ratio of diameters of the insulating particles (D) and the conductive particles (d). This is described by the following equation:

$$V_c = 100\left[\frac{1}{1 + ((4/\theta)(D/d))}\right] \quad (2)$$

where θ is a quantity to describe the arrangement of the conductive particles on the surface of the insulating ones. By lowering the sintering temperatures from 1700 to 1500 °C, the TiN grain size decreased and the Si_3N_4 grain size was affected less by the sintering temperature. This results in a higher diameter ratio (D/d) and thus a lower V_c. Moreover, the percolation equation (Eq. (3)) given by Kirkpatrick [26] predicts that the conductivity (σ) of a composite consisting of insulating and conductive particles depends on the amount of the conductive phase above the percolation concentration ($V - V_c$).

$$\sigma = \sigma_o(V - V_c)^s \quad (3)$$

where σ_o is the conductivity of the conductive phase, V the volume fraction of the conductive particles, s the exponent determining the power of the conductivity increase above V_c. The value of ($V - V_c$) increases when decreasing the sintering temperatures from 1700 to 1500 °C because the percolation threshold (V_c) decreases and the volume fraction of the conductive phase (V) is constant (30 vol.%). This results in the increase in conductivity or the decrease in resistivity. Further decreasing the hot-pressing temperature to 1400 °C leaded to an increase in resistivity, which is associated to the low density of this material (78.0% of the theoretical one) and the presence of a high volume fraction (22 vol.%) of pores interrupting the conductive network. The effective volume fraction of TiN, the

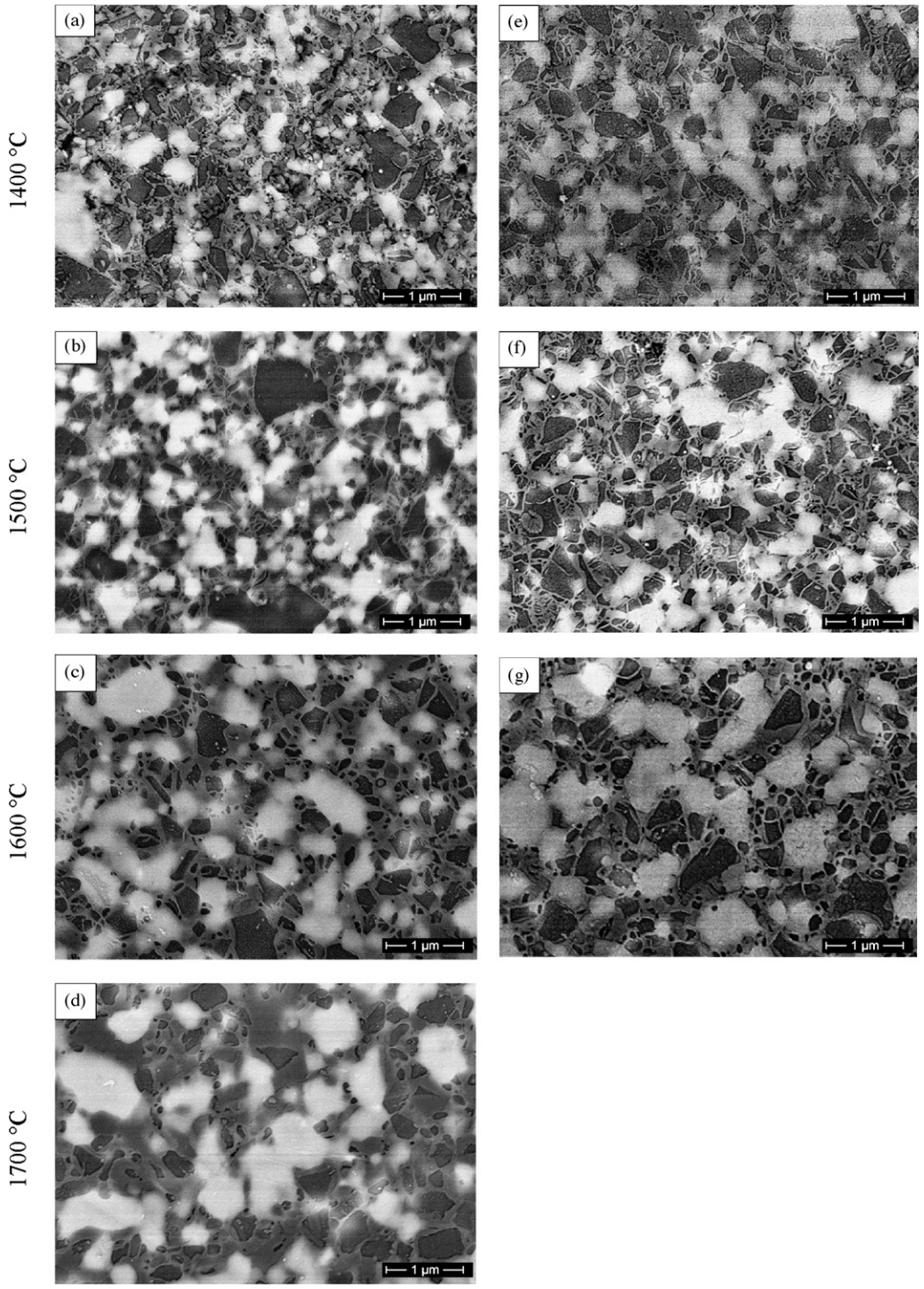

Fig. 6. Backscattered SEM micrographs of Si_3N_4/30 vol.% nano-TiN sintered by HP at 1400 °C (a), 1500 °C (b), 1600 °C (c), 1700 °C (d); and by SPS at 1400 °C (e), 1500 °C (f) and 1600 °C (g). The bright shiny parts represent the TiN phase and the dark ones are the Si_3N_4 phase.

conductor, is only 23.4 vol.% when the pores are considered as an additional non-conductive phase in the material.

A similar trend is also observed in the SPS specimens. However, the specimens SPSed at 1500 and 1600 °C have significantly higher electrical resistivity compared with the HP specimens. This is related to the difference in microstructure. Firstly, the grain sizes of TiN phase of the SPS specimens are larger than those of HP samples, as shown in Fig. 7. For example, when consolidated at 1600 °C, the TiN grain size of the SPS sample (0.53 μm) is approximately 29% larger than that of the HP sample (0.41 μm). This results in a higher resistivity in the SPS samples. The electrical resistivity of TiN (3.34×10^{-5} Ω cm) [1] is in the range of metallic materials. Therefore one can expect that its sintering mechanisms in SPS may be similar to those of metallic materials, including direct generation of heat by the current passing through the sample,

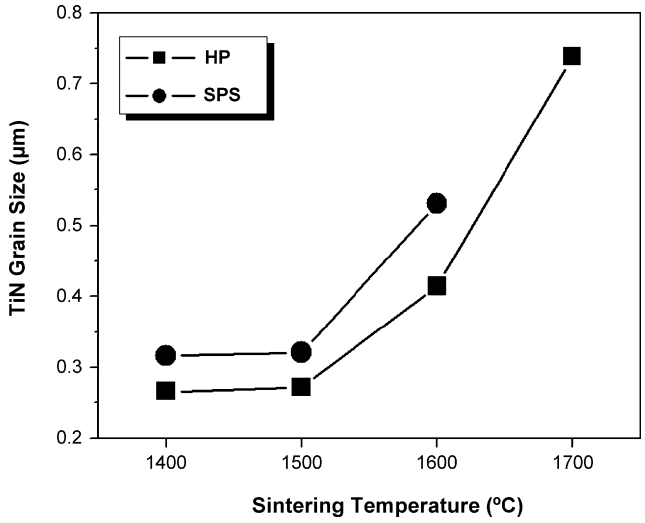

Fig. 7. Grain size of TiN phase vs. sintering temperatures of Si_3N_4/30 vol.% nano-TiN sintered by HP and SPS.

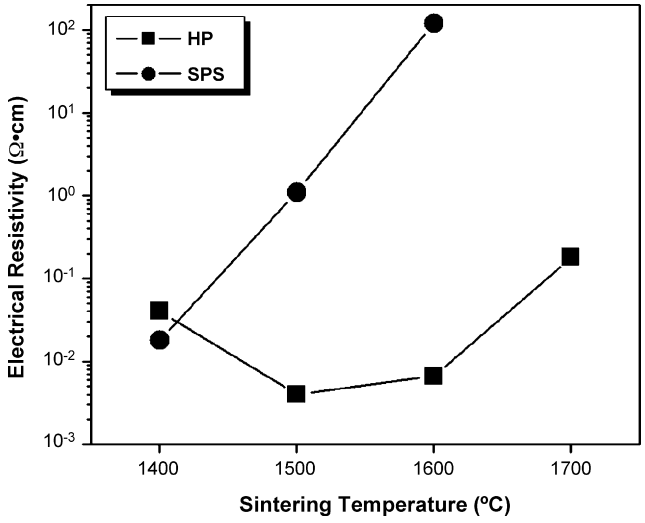

Fig. 8. Electrical resistivity vs. sintering temperature of Si_3N_4/30 vol.% nano-TiN sintered by HP and SPS.

plasma or discharge generation and related surface cleaning [27]. This might contribute to the difference in microstructure of the TiN phase in HP and SPS samples. Moreover the TiN grains in the SPS sample (Fig. 6g) look more globular and tend to be more isolated from each other in comparison with those in the HP sample (Fig. 6c), where more interlinked small TiN grains are visible.

Secondly, the electrical resistivity of the composites is also influenced by the grain boundary phase. Fig. 9 shows the TEM micrographs of the samples synthesized at 1600 °C by HP and SPS, respectively. Si_3N_4 grains appear brighter and TiN particles appear darker. The selected area diffraction (SAD) on the triple junction regions, as indicated with arrows in the TEM micrographs, reveals that the grain boundary phase of the HP sample is amorphous (Fig. 9a). In contrast, partially crystallized grain boundary phase was observed in the SPS specimen (Fig. 9b). The reason of the crystallisation of the grain boundary phase in SPS process is not clear. However it has been shown that the presence of glassy boundary phase in ceramic insulators can reduce electrical resistivity significantly [28]. It is because the glassy phase generally has lower resistivity due to the higher mobility of the ions present in the glass. For example, the resistivity of Al_2O_3 decreases with the amount of impurity and glassy phase. An 99.9% pure Al_2O_3 material has a resistivity of $\sim 10^{15}\ \Omega$ cm and the resistivity decreases to $\sim 10^{11}\ \Omega$ cm at 99.5% purity due to the increase of the amount of glassy boundary phase [28]. Therefore the crystallisation of the grain boundary phase in SPS sample may contribute to the higher resistivity. Furthermore there may be an influence of the grain boundary thickness on conductivity. However, this requires further TEM investigation. Moreover it seems that the presence of crystallized grain boundary phase in SPS sample may restrict morphology development of TiN phase and the direct contact of the neighbouring TiN grains are more difficult, which leads to a more isolated TiN grain structure. These two reasons may explain why there is four orders of magnitude difference in resistivity of these two materials, which have the same composition, but were processed by different techniques.

Furthermore, the uncertainty in the temperature measurement during the SPS process, due to the inhomogeneous

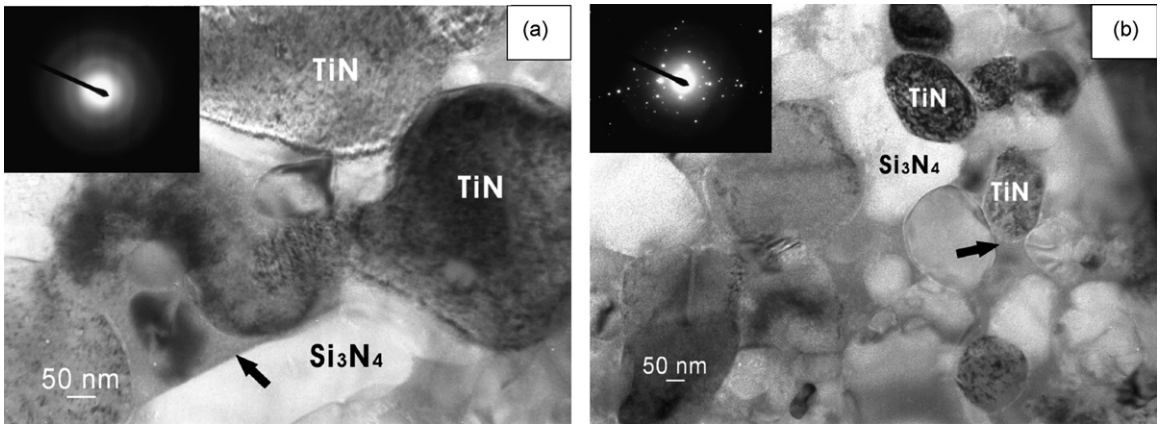

Fig. 9. TEM micrographs of Si_3N_4/30 vol.% nano-TiN composites sintered by: (a) HP and (b) SPS, respectively, with inserted SAD patterns of the grain boundary area as indicated with arrows in the micrographs.

temperature distribution in graphite die, might be also related to the microstructural characteristics in SPS samples. In a study of Dobedoe et al. [15], it was estimated, from the temperature-microstructure relationship, that the temperature at the centre of the specimen could be 230 °C higher than that on the surface of the SPS graphite die at sintering temperature of 1400 °C. It should be pointed out that, in our SPS experiments, the temperature was monitored with an optical pyrometer that was focussed on the bottom of a vertical 'non-through' hole in the upper graphite punch, very close to the specimens. This setup should significantly eliminate the uncertainty induced by the temperature gradient in the graphite die and improve the accuracy of the temperature measurement. According to the finite element simulation of this setup by Vanmeensel et al. [29], the maximal temperature differences between the centre of the samples and focus point of pyrometer are 5 and 2 °C for conductive and insulating samples, respectively.

4. Conclusions

Electroconductive nano-sized TiN dispersed Si_3N_4 composites can be rapidly consolidated to high densities (>98%) by both HP and SPS. A small difference in grain size of TiN phase is observed between these two methods when the same sintering temperature is used. SPS process gives slightly larger TiN grains. In addition, SPS results in crystallisation of the grain boundary phase. The electrical resistivity of the samples sintered at 1600 °C by HP and SPS differs for four orders of magnitude. It is believed that the difference is due to the larger TiN grain size and the crystallisation of the grain boundary phase in SPS sample.

Acknowledgements

The authors would like to express hearty thanks to Dr. Patscheider and Dr. Müller for their assistance on plasma etching. Special thank goes to Dr. Buchser for his help on TEM observation. This research was financially supported by CTI, Switzerland under TopNano21 project–HITCLES (NO. 6620.1).

References

[1] Y.G. Gogotsi, Review: particulate silicon nitride based composite, J. Mater. Sci. 29 (1994) 2541–2556.
[2] J.L. Huang, S.Y. Chen, M.T. Lee, Microstructure, chemical aspects and mechanical properties of TiB_2/Si_3N_4 and TiN/Si_3N_4 composites, J. Mater. Res. 9 (1994) 2349–2354.
[3] Z. Yao, J. Stiglich, T.S. Sudarshan, Molybdenum silicide based materials and their properties, J. Mater. Eng. Perform. 8 (1999) 291–304.
[4] S. Köbel, J. Pluschke, U. Vogt, T.J. Graule, $MoSi_2$–Al_2O_3 electroconductive ceramic composites, Ceram. Inter. 30 (2004) 2105–2110.
[5] G. Blugan, M. Hadad, J. Janszak-Rusch, J. Kuebler, T. Graule, Microstructure, mechanical properties and fractography of commercial silicon nitride-titanium nitride composites for wear applications, J. Am. Ceram. Soc. 88 (2005) 926–933.
[6] S. Balakishnan, J.S. Burnell-Gray, P.K. Datta, Preliminary studies of TiN particulate-reinforced Si_3N_4 matrix composite (Syalon 501) following exposure in oxidising and oxy-chloridising environments, Key Eng. Mater. 99–100 (1995) 279–290.
[7] F. Hong, R.J. Lumby, M.H. Lewis, TiN/Sialon composites via in-situ reaction sintering, J. Eur. Ceram. Soc. 11 (1993) 237–239.
[8] T. Ekstrom, P.-O. Olsson, β-Sialon ceramics with TiN particle inclusions, J. Eur. Ceram. Soc. 13 (1994) 551–559.
[9] Y.G. Gogotsi, F. Porz, The oxidation of particulate-reinforced Si_3N_4–TiN composite, Corros. Sci. 33 (1992) 627–640.
[10] M. Yoshimura, O. Komura, A. Yamakawa, Microstructure and tribological properties of nano-sized Si_3N_4, Scripta Mater. 44 (2001) 1517–1521.
[11] K. Kawano, J. Takahashi, S. Shimada, Highly electroconductive TiN/Si_3N_4 composite fabricated by spark plamsa sintering of Si_3N_4 particles with a nano size TiN coating, J. Mater. Chem. 12 (2002) 361–365.
[12] M. Fricke, R. Nonninger, H. Schmidt, Production of Si_3N_4/TiN nano composites, Adv. Eng. Mater. 2 (2000) 647–652.
[13] A. Bellosi, A. Fiegna, A. Giachello, P.P. Demaestric, Microstructure and properties of electrically conductive Si_3N_4–TiN composite, in: P. Vincenzini (Ed.), Advanced Structural Inorganic Composites, Elsevier Science, Amsterdam, 1991, pp. 225–234.
[14] M. Bracisiewicz, V. Medri, A. Bellosi, Factors inducing degradation of properties after long term oxidation of Si_3N_4–TiN electroconductive composites, Appl. Surf. Sci. 202 (2002) 139–149.
[15] R.S. Dobedoe, F.D. West, M.H. Lewis, Spark plasma sintering ceramics, Bull. Eur. Ceram. Soc. (2003) 19–24.
[16] S. Kawano, J. Takahashi, S. Shimada, The preparation and spark plasma sintering of silicon nitride-based materials coated with nano-sized TiN, J. Eur. Ceram. Soc. 24 (2004) 309–312.
[17] L.J. Van der Pauw, A method of measuring specific resistivity and Hall effect of arbitrary shape, Philips Res. Rep. 13 (1958) 1–9.
[18] D.R. Lide, CRC Handbook of Chemistry and Physics, 83rd ed., CRC Press, Boca Raton, 2002–2003.
[19] L. Gao, J. Li, T. Kusunose, K. Niihara, Preparation and properties of TiN–Si_3N_4 composites, J. Eur. Ceram. Soc. 24 (2004) 381–386.
[20] D.S. Perera, M. Tokita, S. Moricca, Comparative study of fabrication of Si_3N_4/SiC composites by spark plasma sintering and hot isostatic pressing, J. Eur. Ceram. Soc. 18 (1998) 401–404.
[21] W.D. Kingery, Densification during sintering in the presence of a liquid phase. I. Theory, J. Appl. Phys. 30 (1959) 301–306.
[22] EN 623-3, Advanced technical ceramics—Monolithic ceramics-General and textural properties-Part 5: Determination of grain size and grain distribution (characterized by the Linear Intercept Method), 2001.
[23] H.K. Schmidt, The role of TiN in the intergranular phase-forming process in TiN-dispersed Si_3N_4 nanocomposites, J. Am. Ceram. Soc. 88 (2005) 404–410.
[24] L.M. Zivkovic, Z.N. Nikolic, S.M. Boskovic, M. Miljkovic, Microstructural characterisation and computer simulation of conductivity in Si_3N_4–TiN composites, J. Alloy. Compd. 373 (2004) 231–236.
[25] A. Malliaris, D.T. Turner, Influence of particle size on the electrical resistivity of compacted mixtures of polymeric and metallic powders, J. Appl. Phys. 42 (1971) 614–618.
[26] S. Kirkpatrick, Percolation and conduction, Rev. Mod. Phys. 45 (1973) 574–588.
[27] J.R. Groza, A. Zavaliangos, Sintering activation by external electrical field, Mater. Sci. Eng. A287 (2000) 171–177.
[28] M. Bengisu, Engineering Ceramics, Springer, Berlin, 2001.
[29] K. Vanmeensel, A. Laptev, J. Hennicke, J. Vleugels, O. Van der Biest, Modelling of the temperature distribution during the field assisted sintering, Acta Mater. 53 (2005) 4379–4388.